Chemical Reactivity of Pd−Au Bimetallic Nanoclusters Grown via Amorphous Solid Water as Buffer Layer

Elad Gross,[†] Inna Popov,[‡] and Micha Asscher*[,†]

Institute of Chemistry and The Harvey M. Krueger Family Center for Nanoscience and Nanotechnology, The Hebrew University of Jerusalem, Jerusalem 91904, Israel

Received: August 6, 2009; Revised Manuscript Received: September 14, 2009

Bimetallic Pd−Au nanoclusters were prepared on SiO_2/Si(100) via amorphous solid water (ASW) as buffer layer. Selective growth pathways have led to segregated palladium and gold clusters or alloy bimetallic crystallites. Morphology and chemical composition were determined by AFM, SEM, and HR-TEM coupled to EDX analysis. Correlation between clusters morphology and composition to their chemical reactivity is reported for the first time. Temperature programmed reaction studies revealed that conversion of acetylene to ethylene and trimerization to benzene are significantly enhanced over crystalline alloy Pd−Au clusters when compared to clean Pd. A remarkable selectivity toward ethylene formation over benzene is unique to the alloy bimetallic clusters grown via ASW buffer layer on silica, presumably due to suppression of the trimerization pathway. The intrinsic, modified electronic properties of the bimetallic alloy clusters are believed to drive their enhanced chemical reactivity when compared with the pure Pd clusters.

1. Introduction

Supported bimetallic nanoclusters have been at the focus of interest for decades due to their unique catalysis. Their reactivity is dictated by chemical composition, since the addition of a second metallic element often modifies the stability and catalytic activity of the pure metal cluster by affecting both geometry and electronic properties.[1−6] Extended single crystals and gold particles decorated by palladium atoms have shown enhanced catalytic reactivity (per palladium atom) compared to pure predominantly (111) oriented palladium clusters. This was demonstrated for a variety of reactions. A partial list includes vinyl acetate (VA) synthesis,[7] olefins and acetylene hydrogenation,[8,9] and acetylene cyclization to benzene.[10−12] Since the first report on the trimerization reaction of acetylene to benzene by Tysoe et al.,[10] this reaction is considered structure sensitive with the Pd(111) facet the most active. A critical ensemble size of Pd atoms has been postulated as necessary for efficient benzene formation.[12−15] A correlation between electronic structure and catalytic reactivity of bimetallic particles has been proposed theoretically by Nørskov and co-workers. The position (in energy) of the center of d-band electrons with respect to the Fermi level of transition metals is thought to dictate catalytic reactivity of single and bimetallic clusters.[4−6] Clear definition, however, of the dominant factor which governs reactivity of bimetallic clusters, whether structural, purely electronic, or a combination of both, is often rather difficult to obtain.

Model catalysis has been studied in recent decades by in-vacuum deposition of pure metal atoms on oxide surfaces (direct deposition—DD), representing an industrial catalyst.[16−20] Introduction of weakly bound buffer layers to assist the growth of clusters by Weaver and co-workers[21] (buffer layer assisted growth—BLAG) has enabled better control over size and density of particles to obtain more 3D clusters.[21−23]

Here we report on the preparation and initial chemical reactivity of bimetallic clusters, for the first time via the BLAG procedure, manipulating Pd−Au clusters morphology and composition. We were able to demonstrate that the deposition and growth procedure of bimetallic Pd−Au alloy clusters significantly affect their chemical reactivity.

2. Experimental Section

Metal clusters were deposited on SiO_2/Si(100) substrates using amorphous solid water (ASW) as the buffer material all within a UHV chamber equipped with standard surface cleaning and characterization capabilities. SiO_2/Si(100) samples were attached to a stainless steel foil connected to a liquid nitrogen dewar via copper feed throughs and two tantalum rods. A W26%Re−W5%Re thermocouple was spot-welded to the back side of the stainless steel foil. The actual silicon surface temperature was calibrated against multilayer water desorption at 165 K at a heating rate of 3 K/s. Au and Pd atoms were deposited by a resistively heated tungsten filament wrapped around the Au or Pd 99.99% pure wires, employing in situ quartz microbalance (QMB) to determine deposition rates (1.2 ± 0.1 Å/min). Temperature programmed reaction (TPR) measurements were performed following adsorption of 2 L C_2H_2 (1 L = 10^{-6} torr·s) using a quadruple mass spectrometer (QMS) (SRS-200). Ex-situ AFM and HR-SEM were used to determine clusters height and diameter, respectively.[22] BLAG metallic nanoclusters were grown also on top of a standard amorphous carbon (a-C) TEM sample holder grid attached in place of the silicon samples. Their structure and elemental composition were determined using HR-TEM (Tecnai F20 G^2, nominal line resolution 0.1 nm with EDX capability).

3. Results and Discussion

3.1. Pd−Au Clusters Structural Characterization. Pd−Au clusters were prepared by three different pathways. In procedure A bimetallic clusters were grown via two consecutive BLAG cycles: First was the deposition of 2 Å of Pd (metal dosage

* Corresponding author. E-mail: asscher@chem.ch.huji.ac.il.
[†] Institute of Chemistry.
[‡] The Harvey M. Krueger Family Center for Nanoscience and Nanotechnology.

10.1021/jp907614p CCC: $40.75
Published on Web 09/29/2009

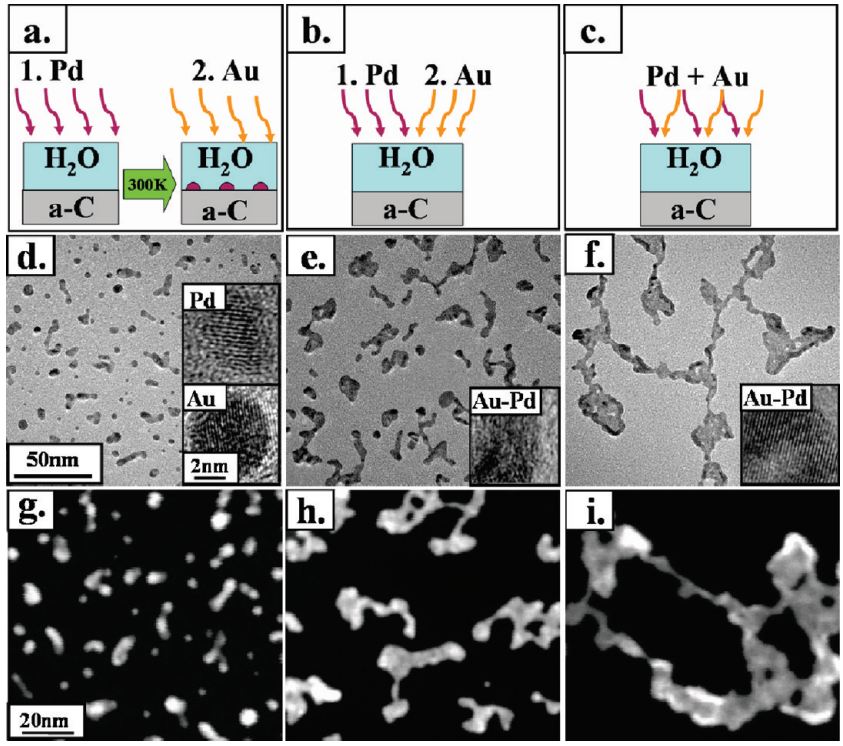

Figure 1. Pd−Au clusters prepared by three different methods. (A) Two consecutive BLAG procedures on 100 ML ASW at 120 K as buffer, the first with Pd, the second with Au (type A clusters, Figure 1a). (B) Evaporation of palladium first and then of gold on top of the same ASW buffer layer (type B clusters (b)). (C) Simultaneous evaporation of gold and palladium on top of the same ASW buffer layer (type C clusters (c)). TEM images of type A, B, and C clusters are shown in (d), (e), and (f), respectively; HR-TEM atom resolved images are shown in the respective insets. STEM images of type A, B, and C clusters are presented in (g), (h), and (i), respectively.

was determined by in situ Quartz Micro Balance), while the second cycle was 2 Å of Au. In both cases ASW was the buffer layer (100 ML) at 120 K on a SiO_2/Si(100) substrate. Annealing the sample to 180 K between the two BLAG cycles results in deposition of the gold clusters on a substrate that is already covered by palladium particles (procedure as in Figure 1a). The second procedure involves consecutive evaporation of 2 Å of gold and 2 Å of palladium on top of the same buffer layer, without intermittent annealing (preparation procedure B; schematic procedure is shown in Figure 1b). Simultaneous evaporation of 2 Å of gold and 2 Å of palladium on top of the same buffer layer is the third mode of preparation—clusters type C (procedure in Figure 1c). HR-TEM images of the metallic nanoparticles prepared by procedures A, B, and C following deposition on amorphous carbon (a-C) TEM sample holder are presented in Figures 1d, 1e, and 1f, respectively.

a-C substrates were specifically studied and compared to silica surfaces addressing a potential influence of these substrates on clusters morphology. It was concluded that these surfaces do not have any effect on the shape and stability of metallic nanoclusters deposited on them.[24]

Procedure A has led to the formation of well separated and nicely resolved particles, while methods B and C produced significantly more aggregated and ramified clusters. This structural difference can be explained by the fact that in methods B and C the total amount of deposited metal on the same ASW buffer layer is twice as large as that of each of the steps of procedure A. Increasing the dosage of evaporated metal on the buffer layer modifies the clusters morphology and enhances the formation of elongated, often branched and ramified structures.[22,23]

The lattice structures of gold and palladium crystallites for type A samples (Figure 1d, inset) were determined using HR-TEM with interplane separation of 2.36 ± 0.03 and 2.23 ± 0.03 Å for Au and Pd. These values correlate well with the lattice constants of Au(111) and Pd(111) crystallites, respectively. Similar analysis performed for type C clusters revealed an intermediate value of 2.29 Å (inset of Figure 1f), which nicely correlates with the preparation of 1:1 elemental composition of these clusters. Type B clusters, in contrast, were predominantly amorphous at 300 K (Figure 1e). This can be explained by the formation of separated, pure seed clusters of Pd (first) and then Au on the same buffer. Evaporation of the ASW buffer and subsequent heating to room temperature is apparently not enough to form well ordered crystallites. Annealing of type B clusters to 450 K in vacuum prior to TEM analysis enables crystallization with interplane separation of 2.28 Å, typical to bimetallic Pd−Au crystalline alloy, practically identical to the way clusters of type C grow already at 300 K.

Further support for structural analysis of the clusters comes from XRD measurements. Clusters of type A diffract at 38.2° and 40.1° that well correlate with Au(111) and Pd(111), respectively (Figure 2a). Peak intensities (weaker for Pd) may reflect differences in the clusters shape (Au clusters are typically higher, more 3D than Pd). A single diffraction peak at 38.7° was obtained from type C clusters, attributed to the formation of crystalline bimetallic alloy (Figure 2c). In contrast, no XRD signal was detected from type B clusters (Figure 2b). Annealing these clusters up to 450 K, on the other hand, has led to the emergence of an XRD signal at 38.8°, suggesting gradual crystallization of the Pd−Au alloy, as discussed above (Figure 2, inset).

Scanning TEM (STEM) images of clusters prepared by the three different methods are shown in Figures 1g−i. TEM and STEM scans reveal changes in the contrast of the different clusters, correlated either with differences in clusters height or modifications in the clusters composition. Gold clusters are

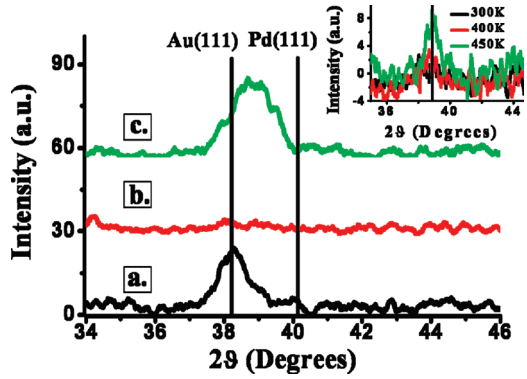

Figure 2. XRD diffraction obtained from clusters of type A (2a), B (2b), and C (2c). Inset: XRD of type B clusters following annealing to the indicated temperatures.

brighter in STEM than palladium clusters as a result of their different atomic numbers.[25,26]

Elemental analysis of a single (typical) cluster (along the red line marked in the STEM images) using the STEM-EDX mode revealed the role of preparation mode on clusters composition and shape. Clusters of type A (Figure 3a) include bright spots that are predominantly composed of gold atoms, located on top of dim, elongated palladium clusters (that were deposited first) (Figure 3d). EDX analysis of C-type clusters (Figure 3c) displays a homogeneous, constant proportion between gold and palladium along the entire line scan (Figure 3f). Here, the contrast changes are correlated with thickness variation of the clusters rather than elemental composition. STEM and EDX measurements of B-type clusters (Figure 3b and 3e), on the other hand, demonstrate only partial overlap in density of Au and Pd.

This isolated cluster compositional analysis has led us to conclude that method A generates essentially separate, segregated gold and palladium particles while Pd−Au crystalline alloy clusters are formed by procedure C. B type clusters that are formed from separate, pure seed clusters of Pd and Au were not fully merged to form crystalline alloy upon annealing to room temperature.

AFM images of type A, B, and C clusters are shown in Figures 4a−c, respectively. Height distribution analysis of the three samples is shown in Figure 4d. In Figure 4a one can clearly distinguish between the bright spherical clusters and the dimmer elongated ones. Analysis of the clusters size revealed a bimodal distribution with two height maxima, at 7 and 12.5 nm (Figure 4d, line a). The average height of pure Pd and Au clusters prepared by a single BLAG cycle (of 2 Å on 100 ML of H_2O) was 5 and 13 nm, respectively. The bright and higher clusters shown in Figure 4a are therefore attributed to gold clusters, while the dimers and lower ones are palladium. These results further support the conclusion based on STEM-EDX measurements that mostly individual, separate Au and Pd clusters are formed by preparation method A. Elongated clusters constructed from several clusters that have aggregated to form up to 100 nm long chains were the result of preparation method B (Figure 4b). Kinetic limitations prevent full merging and fusion of the aggregated clusters. Height analysis of this sample reveals that the average height of the clusters is 8 ± 2 nm (Figure 4d, line b). Type C clusters grow as long wires, but the individual seed clusters cannot be distinguished so well (Figure 4c). Codeposition of Au and Pd on the ASW film in procedure C results in partial merge and fusion of the elements. The formation of larger seed clusters leads to smoother and higher (10 nm on average) wires (Figure 4c and Figure 4d, line c).

Supporting evidence is also obtained from UV−vis absorption measurements of the different types of clusters grown on sapphire substrate (Figure 5). The intensity of the surface plasmon resonance of gold decreases and the peak position is blue-shifted upon changing the preparation procedure from A to B to C. These modifications strengthen the conclusion that preparation method C leads to the formation of crystalline bimetallic alloy, expected to have its surface plasmon resonance shifted way to the UV range.[26]

3.2. Chemical Reactivity of Pd−Au Clusters. BLAG clusters have so far been studied mostly for their structure and growth mechanism, following buffer desorption[21−23,25] with one report addressing CO adsorption capabilities of pure gold BLAG clusters.[27]

Here we present, for the first time, their unique chemical reactivity as model catalysts. The initial reactivity of the three types of nanoclusters has been examined employing temperature programmed reaction (TPR) measurements. Acetylene hydrogenation to ethylene and trimerization to benzene were inves-

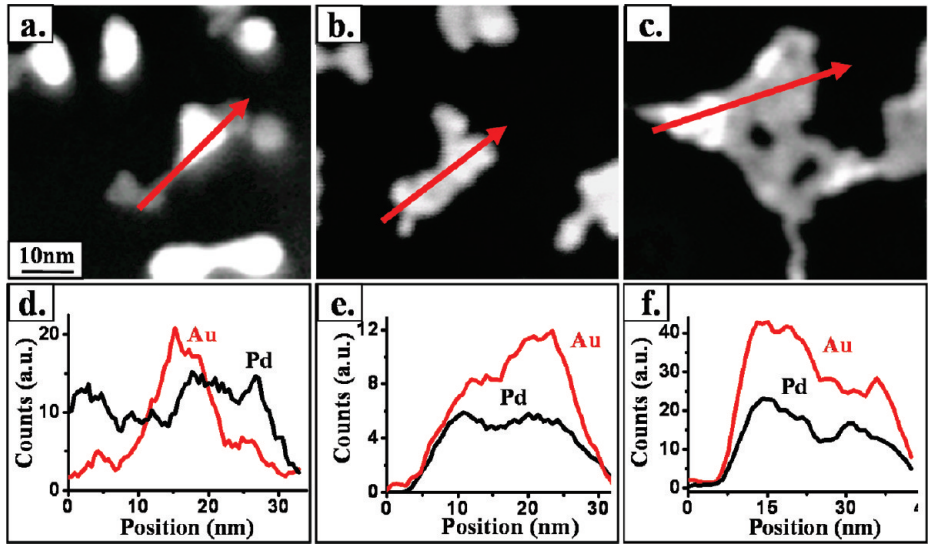

Figure 3. STEM images (a, b, and c) and EDX analysis of gold and palladium elemental distribution across type A, B, and C clusters (d, e, and f), respectively.

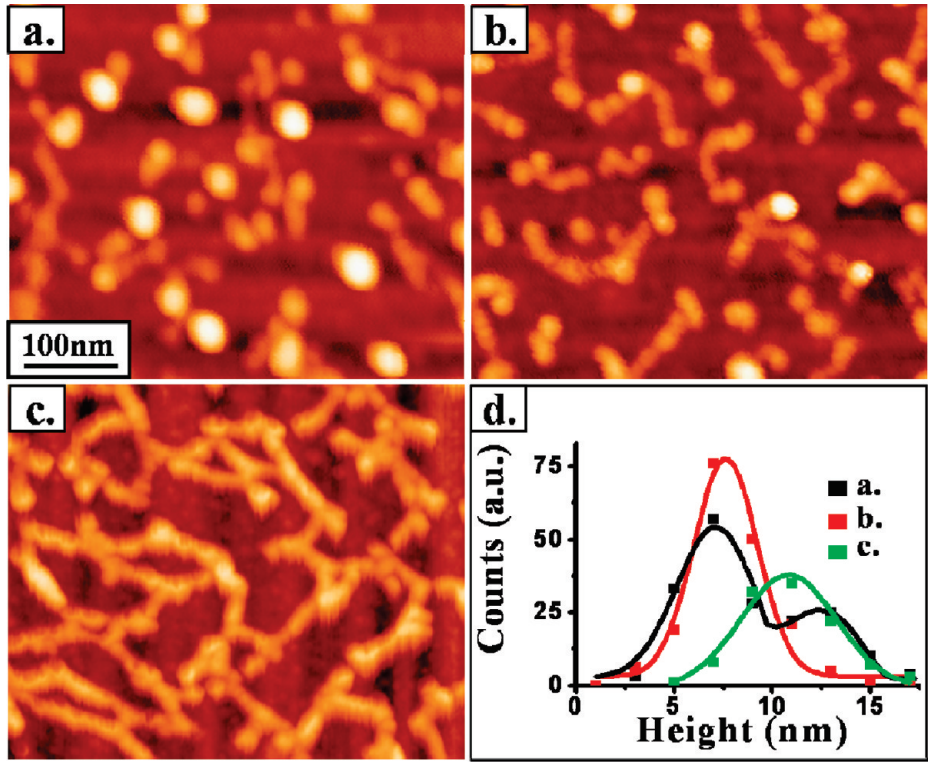

Figure 4. AFM images of type A, B, and C clusters are shown in (a), (b), and (c), respectively. Height distribution analysis of the three types of clusters is shown in (d).

tigated as model reactions. Formation of ethylene following acetylene hydrogenation is the dominant reactivity channel (Figure 6a).

3.2.1. Acetylene Hydrogenation. Preparation methods A, B, and C have enhanced ethylene formation rate by 1.1-, 2.1-, and 3.2-fold, respectively, compared to the yield obtained over pure BLAG Pd clusters. Upon adsorption of acetylene and subsequent TPR, hydrogenation to ethylene takes place as the major reactivity pathway. The question what is the origin of hydrogen atoms necessary for this reaction to take place, whether from neighbor acetylene or from the buffer water molecules, was addressed by substituting the H_2O ASW buffer by D_2O. It was found that at least 60% of the ethylene molecules do not contain deuterium. This observation suggests that ethylene formation mechanism over the Pd−Au clusters proceeds predominantly via acetylene decomposition:

$$HC{\equiv}CH_{(ad)} \xrightarrow{150\ -\ 170\ K} HC{\equiv}C^{\bullet}{}_{(ad)} + H_{(ad)}$$

$$HC{\equiv}CH_{(ad)} + 2H_{(ad)} \rightarrow H_2C{=}CH_{2(ad)} \xrightarrow{170\ -\ 250\ K} H_2C{=}CH_{2(g)}$$

The low temperature dehydrogenation of acetylene (170 K or lower) is inferred from the low temperature onset of ethylene desorption, as seen in Figure 6a.

Clusters growth mechanism via BLAG results in strong interaction of (hot) Pd atoms with H_2O (D_2O) on top of the ASW buffer layer. This leads to some water dissociation that is an additional potential source of hydrogen (deuterium) for the formation of ethylene. Acetylene conversion to ethylene by directly deposited (DD) Pd−Au bimetallic clusters (Figure 6a)

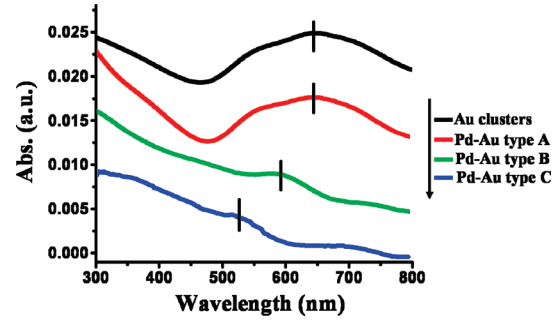

Figure 5. Surface plasmon resonance spectra of gold and type A, B, and C clusters deposited via BLAG on top of 1 mm thick sapphire windows as substrate. Each spectrum is the average of 100 absorption spectra taken by employing a standard UV−vis spectrophotometer.

(and pure Pd), however, where water molecules do not exist, indicates that the contribution to overall ethylene formation from partial water dissociation during BLAG clusters growth cannot be ignored but it is limited to less than half of the total yield.

It is interesting to compare the formation of ethylene from acetylene discussed here to earlier reports on acetylene reactivity over extended Pd/Au(111) and Au/Pd(111) surfaces[12] and the reactivity of pure Pd clusters directly deposited on Al_2O_3 planar oxide surface.[13] The Pd/Au(111) substrate does not seem to catalyze ethylene formation at all, while on the Au/Pd(111) substrate only a very small amount of ethylene was detected in TPR measurements. In both surfaces the major and predominant product was benzene, the result of acetylene trimerization. In contrast, the Pd/Al_2O_3 surface catalyzes the formation of ethylene (TPR detection of mass 28 in ref 13) at comparable yield to benzene.

As further discussed below, BLAG Pd−Au bimetallic clusters are remarkably selective toward ethylene formation over benzene, unlike the extended metallic Pd and Au substrates. Acetylene conversion to ethylene is more than 2 orders of

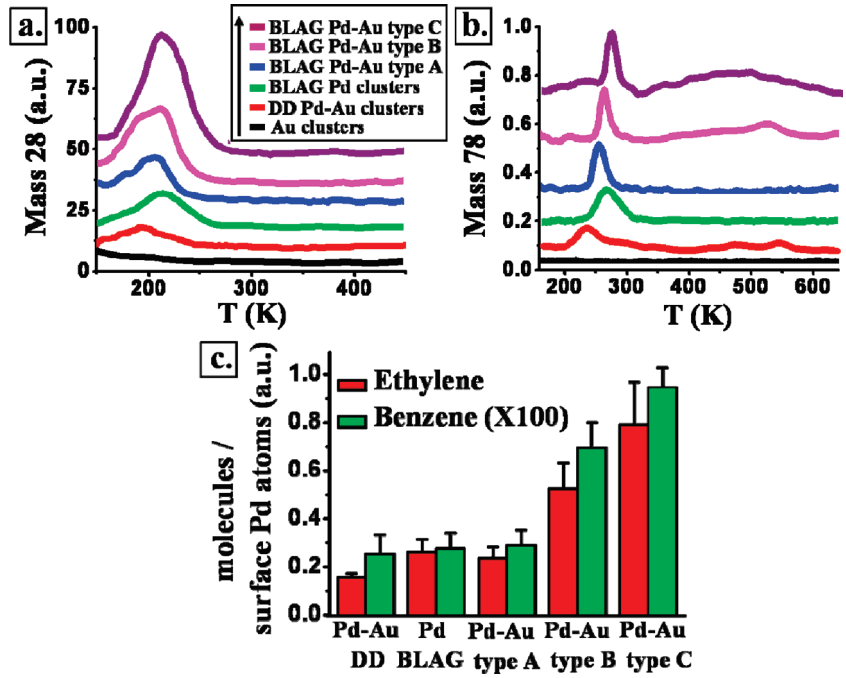

Figure 6. TPR of ethylene (mass 28) (a) and benzene (mass 78) (b) signals collected following adsorption of 2 L C_2H_2 on the different clusters at 120 K; heating rate was fixed at 3 K/s. Calculation of the relative amount of desorbed product molecules per surface Pd atoms for the different clusters (c).

magnitude faster than its trimerization to benzene (compare Figures 6a and 6b). Regarding the origin of this unique selectivity, one may ask if benzene formation is inhibited over bimetallic BLAG clusters or if it is the hydrogenation reaction to form ethylene that is significantly enhanced. Reactivity study over thick layers (4−5 ML) of directly deposited, pure Pd over the SiO_2/Si(100) substrate (not shown) reveals relatively minor change in the yield of hydrogenation reaction to form ethylene, but a dramatic enhancement in the trimerization reaction of acetylene to form benzene.

We conclude, therefore, that the main difference between BLAG clusters and extended Pd/Au(111) and Au/Pd(111) substrates is the suppression of the trimerization reaction over BLAG clusters.

3.2.2. Acetylene Trimerization to Benzene. The TPR spectra of benzene (mass 78) acquired following 2 L acetylene adsorption on cluster types A, B, and C are shown in Figure 6b. Adsorption of acetylene on pure gold clusters has not led to any ethylene or benzene formation, while a single benzene desorption peak was obtained from pure Pd/BLAG clusters. Similar results were detected on Pd−Au clusters prepared by type A procedure. Type B clusters have led to higher intensity of the low temperature benzene peak (at 270 K) and to the formation of a new broad high temperature peak centered at ∼500 K. Alloy clusters of type C were found most reactive, in particular at the high temperature range. The ∼270 K peak presumably corresponds to reactively formed weakly adsorbed and tilted benzene molecules, formed from high coverage acetylene. The high temperature peak (450−550 K) is associated with desorption of flat laying benzene,[10,12] expected at low coverage. These two benzene desorption sites were originally identified on top of extended Pd(111) single crystal surface.[10] The addition of gold changed not only the TPR profile but also the overall benzene formation yield. Total uptake measurements indicate that acetylene trimerization reaction rates are 1-, 2.5-, and 4.2-fold faster (normalized to the reactivity over pure BLAG Pd clusters) for types A, B, and C, respectively. The variation in chemical reactivity can be attributed to the degree of metal intermixing and formation of Pd−Au alloy. Type A clusters are characterized by separate gold (nonreactive) and Pd clusters; therefore, their reactivity is practically identical to pure Pd. In contrast, type B and C samples possess gradually more bimetallic alloy character that is the most chemically active. The emergence of high temperature benzene TPR peak (∼500 K) suggests that Pd−Au alloy clusters stabilize strongly bound benzene molecules. This peak was not observed on pure Pd clusters presumably because stronger interaction with the clean palladium may have led to decomposition of intermediates such as vinylidene ($H_2C{=}C{-}M$) prior to benzene formation.[12]

The unique reactivity of BLAG Pd−Au alloys was calibrated against directly deposited (DD) bimetallic clusters having the same composition. In both hydrogenation and trimerization reactions of acetylene, the B and C type BLAG samples were at least three times more reactive than the DD clusters. This observation is further substantiated when reactivity is normalized to (estimated) surface exposed Pd atoms (Figure 6c). Interestingly, similar selectivity toward ethylene production described here for the BLAG Pd−Au bimetallic clusters was reported also for similar clusters sizes of Au−Pd/TiO_2 catalysts prepared by redox wet preparation methods.[9]

Suppression of the benzene formation pathway relative to ethylene formation by small, wires-like bimetallic clusters formed via the BLAG method (Figure 4) can be explained by the lack of extended (111)-like surfaces of Pd or Au−Pd, the ensemble effect. Focusing on the benzene formation, however, one clearly realizes the reactivity enhancement, presumably due to electronic effect of low temperature bimetallic alloy formation in the BLAG procedure. Similar alloying effects on extended Au/Pd(111) and Pd/Au(111) surfaces were demonstrated following high temperature annealing.[12]

4. Conclusions

Measurements performed on isolated bimetallic particles and ensemble of clusters have verified that careful tuning of BLAG

clusters preparation procedure may lead to low temperature Pd−Au alloy formation. Chemical reactivity studies are reported here for the first time employing BLAG particles as model catalysts. Significantly enhanced reaction rates for the conversion of acetylene to ethylene and trimerization to benzene by the BLAG bimetallic clusters were measured compared to the reactivity of pure Pd clusters under identical conditions. Very high selectivity toward acetylene decomposition and subsequent ethylene formation has been reported with only less than 2% of products channeled to benzene formation. Relative suppression of benzene formation over ethylene is explained in terms of the lack of sufficiently extended hexagonal Pd planes within the typical morphology of BLAG clusters, consistent with the well-known ensemble effect favoring Pd(111) planes for catalyzing benzene formation. Focusing on the effect of clusters composition and morphology on ethylene and benzene formation, our results are in qualitative agreement with electronic structure modification of the bimetallic alloy clusters compared with clean Pd or Au particles. This theory, suggested by Nørskov and co-workers,[4,5] is based on d-band electrons energy that change as the fraction of gold atoms increases. This effect explains higher thermal stability of intermediates that leads to new, high temperature reactivity pathways, e.g., for benzene formation.

Acknowledgment. Acknowledgement is made to the donors of the American Chemical Society Petroleum Research Fund for partial support of this research. The support of the US−Israel Binational Science Foundation and the Israel Science Foundation is acknowledged. E.G. is grateful for a generous fellowship given by The Eshkol Foundation, administered by Israel Ministry of Science.

References and Notes

(1) Chen, J. G.; Menning, C. A.; Zellner, M. B. *Surf. Sci. Rep.* **2008**, *63*, 201.
(2) Rodriguez, J. A. *Surf. Sci. Rep.* **1996**, *24*, 223.
(3) Studt, F.; Abild-Pedersen, F.; Bligaard, T.; Sorensen, R. Z.; Christensen, C. H.; Nørskov, J. K. *Science* **2008**, *320*, 1320.
(4) Nørskov, J. K.; Bligaard, T.; Rossmeisl, J.; Christensen, C. H. *Nat. Chem.* **2009**, *1*, 37.
(5) Hammer, B.; Nørskov, J. K. *Adv. Catal.* **2000**, *45*, 71.
(6) Kitchin, J. R.; Nørskov, J. K.; Barteau, M. A.; Chen, J. G. *Phys. Rev. Lett.* **2004**, *93*, 156801.
(7) Chen, M. S.; Kumar, D.; Yi, C. W.; Goodman, D. W. *Science* **2005**, *310*, 291.
(8) Sarkany, A.; Geszti, O.; Safran, G. *Appl. Catal., A* **2008**, *350*, 157.
(9) Choudhary, T. V.; Sivadinarayana, C.; Datye, A. K.; Kumar, D.; Goodman, D. W. *Catal. Lett.* **2003**, *86*, 1.
(10) Tysoe, W. T.; Nyberg, G. L.; Lambert, R. M. *Surf. Sci.* **1983**, *135*, 128.
(11) (a) Baddeley, C. J.; Ormerod, R. M.; Stephenson, A. W.; Lambert, R. M. *J. Phys. Chem.* **1995**, *99*, 5146. (b) Baddeley, C. J.; Tikhov, M.; Hardacre, C.; Lomas, J. R.; Lambert, R. M. *J. Phys. Chem.* **1996**, *100*, 2189.
(12) Storm, J.; Lambert, R. M.; Memmel, N.; Onsgaard, J.; Taglauer, E. *Surf. Sci.* **1999**, *436*, 259.
(13) Holmblad, P. M.; Rainer, D. R.; Goodman, D. W. *J. Phys. Chem. B* **1997**, *101*, 8883.
(14) Gentle, T. M.; Muetterties, E. L. *J. Phys. Chem.* **1983**, *87*, 2469.
(15) Abbet, S.; Sanchez, A.; Heiz, U.; Schneider, W. D. *J. Catal.* **2001**, *198*, 122.
(16) Baumer, M.; Freund, H. J. *Prog. Surf. Sci.* **1999**, *61*, 127.
(17) Lai, X.; St Clair, T. P.; Valden, M.; Goodman, D. W. *Prog. Surf. Sci.* **1998**, *59*, 25.
(18) Heemeier, M.; Carlsson, A. F.; Naschitzki, M.; Schmal, M.; Baumer, M.; Freund, H. J. *Angew. Chem., Int. Ed.* **2002**, *41*, 4073.
(19) Yi, C. W.; Luo, K.; Wei, T.; Goodman, D. W. *J. Phys. Chem. B* **2005**, *109*, 18535.
(20) Luo, K.; Wei, T.; Yi, C. W.; Axnanda, S.; Goodman, D. W. *J. Phys. Chem. B* **2005**, *109*, 23517.
(21) Huang, L.; Chey, S. J.; Weaver, J. H. *Phys. Rev. Lett.* **1998**, *80*, 4095.
(22) Gross, E.; Horowitz, Y.; Asscher, M. *Langmuir* **2005**, *21*, 8892.
(23) Waggoner, P. S.; Palmer, J. S.; Antonov, V. N.; Weaver, J. H. *Surf. Sci.* **2005**, *596*, 12.
(24) Schmidt, A. A.; Eggers, H.; Herwig, K.; Anton, R. *Surf. Sci.* **1996**, *349*, 301.
(25) Gross, E.; Asscher, M. *Phys. Chem. Chem. Phys.* **2009**, *11*, 710.
(26) Ferrer, D.; Torres-Castro, A.; Gao, X.; Sepulveda-Guzman, S.; Ortiz-Mendez, U.; Jose-Yacaman, M. *Nano Lett.* **2007**, *7*, 1701.
(27) Gross, E.; Asscher, M.; Lundwall, M.; Goodman, D. W. *J. Phys. Chem. C* **2007**, *111*, 16197.

JP907614P